

Aerosol Mass yields of selected Biogenic Volatile Organic Compounds – a theoretical study with near explicit gas-phase chemistry

Carlton Xavier¹, Anton Rusanen¹, Putian Zhou¹, Chen Dean¹, Lukas Pichelstofer¹, Pontus Roldin², Michael Boy¹

¹Institute for Atmospheric and Earth Systems Research (INAR), Physics, University of Helsinki

²Division of Nuclear Physics, Lund University, Box 118, SE-22100, Lund, Sweden

5

6 **Correspondence** : Carlton Xavier (carlton.xavier@helsinki.fi), Michael Boy (michael.boy@helsinki.fi)

7

8 **Abstract**

9 In this study we modeled secondary organic aerosols (SOA) mass loadings from the oxidation (by O₃,
10 OH and NO₃) of five representative Biogenic Volatile Organic compounds (BVOCs): isoprene, endocyclic
11 bond containing monoterpenes (α -pinene and limonene), exocyclic double bond compound (β -pinene) and a
12 sesquiterpene (β -caryophyllene). The simulations were designed to replicate idealized smog chamber and
13 oxidative flow reactors (OFR). The master chemical mechanism (MCM) together with the peroxy radical
14 autoxidation mechanism (PRAM), were used to simulate the gas-phase chemistry. The aim of this study was
15 to compare the potency of MCM and MCM+PRAM in predicting SOA formation. SOA yields were in good
16 agreement with experimental values for chamber simulations when MCM+PRAM was applied, while a
17 standalone MCM under-predicted the SOA yields. Compared to experimental yields, the OFR simulations
18 using MCM+PRAM over-predicted SOA mass yields for BVOCs oxidized by O₃ and OH, probably owing to
19 increased seed particle surface area used in the OFR simulations. SOA yields increased with decreasing
20 temperatures and NO concentrations and vice-versa. This highlights the limitations posed when using fixed
21 SOA yields in a majority of global and regional models. Few compounds that play a crucial role (>95% of
22 mass load) in contributing to SOA mass increase (using MCM+PRAM) are identified. The results further
23 emphasized that incorporating PRAM in conjunction with MCM does improve SOA mass yields estimation.

24

25 1. **Introduction**

26 Atmospheric secondary organic aerosols, formed from gas to particle phase conversion of the
27 oxidation products of volatile organic compounds (VOC) significantly impact the organic aerosol mass
28 loadings (Griffin, 1999; Kanakidou et al., 2005). However, the scale of SOA contribution to the aerosol
29 particle mass is still subjected to high uncertainties (Hao et al., 2011). The elevated aerosol particle

30 concentrations are shown to have inimical effects on health (Miller et al., 2007), and a varying degree of
31 influence on the climate by forming cloud condensation nuclei (CCN), altering the cloud properties and
32 radiative balance (Rosenfeld et al., 2014; Schmale et al., 2018). Therefore, it is acutely necessary to
33 understand the role and contributions of SOA to the particle loading in the atmosphere. Biogenic VOCs from
34 forest are estimated to contribute to about 90% of VOCs emissions globally (Guenther et al., 1995, 1999 and
35 2000). The most important BVOCs for SOA formation are isoprene (C_5H_8), monoterpenes ($C_{10}H_{16}$) and
36 sesquiterpenes ($C_{15}H_{24}$). These compounds are all alkenes containing at least one carbon-carbon double bond,
37 enabling them to undergo oxidation by the dominant atmospheric oxidants: the hydroxyl radical (OH), ozone
38 (O_3) and the nitrate radical (NO_3). For some of the terpenes, initial oxidation steps can lead to formation of
39 highly oxygenated organic molecules (HOM). These HOMs generally have low volatilities and can condense
40 nearly irreversibly, thereby producing SOA (Ehn et al., 2014). HOMs, detected in both the ambient
41 atmosphere and chamber experiments (Ehn M, et al., 2012) are formed by autoxidation (Berndt et al., 2016;
42 Crouse and Nielsen, 2013) wherein peroxy radicals (RO_2) undergo subsequent intramolecular H-shifts
43 accompanied by rapid reactions with O_2 . Autoxidation hence results in compounds containing multiple
44 functional groups such as hydroxyls, peroxides and carbonyls (Bianchi et al., 2017, Bianchi et al., 2019).

45 A majority of chamber and flow-tube experiments have focused on HOM formation from the
46 oxidation of various VOCs and their contribution to SOA mass loadings (Ehn et al., 2014; Kristensen et al.,
47 2017). Oxidation of isoprene (Liu et al., 2016), endocyclic monoterpenes containing reactive double bonds
48 such as α -pinene and limonene (Zhao et al., 2015), or exocyclic double bond containing compounds such as
49 β -pinene (Jokinen et al., 2015) and sesquiterpenes such as β -caryophyllene (Chen et al., 2012) have been
50 investigated. The SOA forming potential of various BVOCs depends on the isomeric structures (Friedman
51 and Farmer, 2018; Keywood et al., 2004). Ozonolysis of compounds containing reactive endocyclic bonds
52 such as α -pinene produce higher SOA mass yields of 41% in comparison to those with exocyclic bonds (β -
53 pinene), which produce mass yields of 17 % (Lee et al., 2006). One explanation for this dependence on the
54 isomeric structure is attributed to the formation of HOMs (Ehn et al., 2014). Another important factor
55 influencing HOM formation is the initial oxidant, as pointed out by Zhao and co-workers (2015). They
56 showed that the SOA formation by OH oxidation of α -pinene and limonene were lower when compared to
57 their SOA formed by ozonolysis. Further they measured lower H/C ratio for SOA produced by monoterpene
58 ozonolysis (experiments were carried out in dark with CO as OH scavenger), in comparison to OH oxidation
59 of α -pinene and limonene. This was attributed to the formation of RO_2 radicals (monoterpenes + O_3) which
60 undergo internal hydrogen shifts and subsequently react with another RO_2 radical, to form compounds
61 containing carbonyl groups while losing hydrogen atoms in the process. A similar analysis was conducted by

62 Draper et al. (2015), who showed that an increase in NO₂ concentration reduced α-pinene ozonolysis SOA
63 mass yields, while no appreciable reduction in mass yields are reported for β-pinene and Δ³-carene
64 ozonolysis. On the other hand, the mass yields from limonene ozonolysis increased with increasing NO₂
65 concentrations (Draper et al., 2015). This disparity in mass yields for different BVOCs in the presence of NO₂
66 is possibly caused by the formation of high MW oligomers (or lack of in case of α-pinene) through oxidation
67 with NO₃ that contribute to SOA mass loadings (Draper et al., 2015).

68 Due to computational limitations, many regional and canopy scale atmospheric chemistry models
69 generally use isoprene and/or a representative monoterpene (generally α-pinene), to model SOA yields
70 (Friedman and Farmer, 2018). The SOA yields of different monoterpenes vary with structure, NO_x and
71 temperature (Friedman and Farmer, 2018; Kristensen et al., 2017; Presto et al., 2005). This poses a limitation
72 on using representative monoterpene fixed SOA yields in many of the global models and increases
73 uncertainties in predicting cloud condensation nuclei concentrations, cloud droplet number concentrations and
74 radiative balance due to aerosol loading's.

75 This work aims to investigate the SOA mass loading from the oxidation products of BVOCs with the
76 atmospheric oxidants OH, O₃ and NO₃ with a specific focus on the BVOCs isoprene, α-pinene, β-pinene,
77 limonene and β-caryophyllene. Further we study the effect of varying temperature (258.15 K – 313.15 K) and
78 NO concentrations (0 - 5 ppb) on α-pinene oxidation mass yields. We use the master chemical mechanism
79 (MCMv3.3.1) (Jenkin et al., 1997, 2012 and 2015; Saunders et al., 2003), a near explicit gas-phase chemical
80 mechanism together with peroxy radical autoxidation mechanism (PRAM, Roldin et al., 2019) (PRAM +
81 MCM). The aim is to understand the importance and contribution of peroxy radical autoxidation products to
82 the SOA mass yields from terpenes.

83

84 2. Model description

85 2.1 Malte Box

86 MALTE (Model to predict new Aerosol formation in Lower TropospherE) is a one-dimensional
87 model consisting of modules calculating boundary layer meteorology, emissions of BVOCs, gas-phase
88 chemistry and aerosol dynamics with the aim to simulate particle distribution and growth in the lower
89 troposphere (Boy et al., 2006). In this study, a zero-dimensional version, MALTE-Box is applied to simulate
90 an ideal chamber and flow-tube environment (i.e. no wall losses effects are considered in this study). For the

91 simulations performed in this study the emission module was switched off while only employing the gas-
92 phase chemistry and aerosol dynamics module.

93 Kinetic preprocessor (KPP) is used to generate a system of coupled differential equations to solve the
94 gas-phase chemistry schemes (MCM+PRAM, Damian et al., 2002). The peroxy radical autoxidation
95 mechanism (PRAM), (Roldin et al., 2019, Qi et al., 2018, Öström et al., 2017), formulated based on the
96 oxidation of monoterpenes as described by Ehn et al. (2014) was incorporated alongside MCMv3.3.1. PRAM
97 explicitly describes the formation and evolution of peroxy radicals (RO_2) from the ozonolysis and OH
98 oxidation of monoterpenes, driven by subsequent H-shifts and O_2 additions. The current version of PRAM
99 based on experimental and theoretical studies, considers HOM autoxidation for a fraction of the peroxy
100 radicals formed during the ozonolysis of α -pinene and limonene and OH oxidation of α -pinene, β -pinene and
101 limonene. This is achieved by assigning species specific molar yields for the formation of first RO_2 , which
102 subsequently initiates the autoxidation chain (Roldin et al., 2019). Currently, in PRAM a maximum first
103 generation RO_2 yield of 9% for α -pinene ozonolysis, 21.9 % for limonene ozonolysis, 2.5 % for α -
104 pinene+OH, and 1% for both limonene+OH and β -pinene+OH first generation products are allowed to initiate
105 autoxidation (Öström et al., 2017, Qi et al., 2018, Roldin et al., 2019). For β -pinene ozonolysis the molar
106 yield of RO_2 is minor (<0.1 %) (Roldin et al., 2019, Ehn et al. 2014) and hence not considered in this work.
107 The above mentioned RO_2 molar yields used in this work are close to the experimental values obtained in
108 both smog chamber and flow tube experiments. Ehn et al. (2014) measured an RO_2 yield of ~7% for α -pinene
109 ozonolysis and ~17% for limonene ozonolysis, whereas Jokinen et al. (2015) measured 0.58 % and 0.93 % for
110 OH oxidation of β -pinene and limonene respectively. The autoxidation is terminated by bimolecular
111 reactions, wherein the RO_2 formed reacts with NO, HO_2 or other peroxy radicals, thereby forming alkoxy
112 radicals, closed shell monomers or dimers (Roldin et al., 2019). The PRAM considers temperature dependent
113 autoxidation reaction rates, which is important when investigating the SOA mass yields at varying
114 temperatures (Table 1c). It should be noted that the temperature dependence in PRAM is a first of its kind but
115 needs further evaluation using recent measurements of HOM formation at different temperatures (e.g.
116 Quéléver et al.2018).

117 The aerosol dynamics are simulated using the University of Helsinki Multicomponent Aerosol model
118 (UHMA) originally from Korhonen et al. (2004). The model has undergone significant development since
119 then to allow simulation with all the compounds from MCM. It now supports an unlimited number of
120 condensing vapors and solves condensation using the analytical predictor of condensation method from
121 Jacobson (1997). The condensation algorithm considers both, the Kelvin effect and Raoult's law. The
122 processes included in the model are nucleation, condensation, evaporation, coagulation and deposition. The

123 discretization of the size distribution and the time evolution is modeled with the moving section approach,
124 with optional redistribution to a fixed grid. In this work, the redistribution is active to make the coagulation
125 more accurate, since it requires that grid points are available near the size of the coagulated particles. In this
126 study nucleation and deposition are not active, and hence are not considered. A total of 100 size bins ranging
127 from 1nm to 20 μ m with the fixed grid was applied for this study.

128 A group contribution method based on Nannoolal et al. (2008) using the UManSysProp online system
129 (Topping, 2016) was used to estimate the pure liquid saturation vapor pressures (p_0) of the organic
130 compounds in MCMv3.3.1. For the PRAM species, p_0 were estimated using the functional group method
131 SIMPOL (Pankow and Asher, 2008; see Roldin et al., 2019 for details)

132 2.2 Simulations

133 The simulations performed in this study are aimed to closely resemble an idealized smog chamber
134 (batch mode setup) and an Oxidative Flow Reactor (OFR) without interactions between the gas phase and the
135 system walls. For the chamber runs, the VOC and oxidants were introduced at the beginning (time, $t=0$ sec),
136 set to certain concentrations and then allowed to react. Both chamber and OFR simulations are performed
137 using ammonium sulfate seed particles which are introduced at time $t=0$. The condensation sink (CS) was
138 inferred from the size distribution of seed particles used in the model. The CS for the chamber and OFR
139 simulations was set to 0.00067 s^{-1} and 0.067 s^{-1} respectively. SOA mass yields obtained using an OFR are
140 sensitive to short residence time used, hence the seed particle surface area should be chosen in order to
141 overcome the mass yield underestimation (Ahlberg et al., 2019). CS sensitivity runs (Supplement Figure S1)
142 were performed for α -pinene- O_3 to determine the CS for which there are no appreciable change in mass yields
143 with increasing particle surface.

144 The simulation for the chamber setup is run for a maximum time of 24 hours and ends when either of
145 the 2 criteria are satisfied: (1) the simulation time reaches the 24-hour mark or (2) 90 % of the initial
146 precursor VOC has reacted away. In the latter case the simulation is continued for an additional 2 hours to
147 ensure enough time for the vapors to condense onto the seed particles. On the contrary, the OFR runs were
148 simulated for a maximum residence time of 100 seconds, ensuring all initial precursor vapors were oxidized.
149 Seed particles were also added in the OFR simulations. The oxidant concentrations used for the OFR
150 simulations are significantly higher in comparison to the simulated chamber runs (~ 2 orders of magnitude
151 larger). The time step for the chamber and flow-tube simulations are set to $t=10\text{ s}$ and $t=0.1\text{ s}$ respectively.
152 The runs performed were oxidant specific (i.e. VOCs would be oxidized by only one specific oxidant at any

153 given time). For the O₃ specific simulations no OH could form in both, OFR and chamber setups, thus
 154 enabling oxidation of O₃ to be the only pathway.

155 The simulations were performed at atmospheric relevant NO_x (NO_x = NO +NO₂) concentrations,
 156 corresponding to [NO]=0.5 ppb and [NO₂] = 2.0 ppb conditions with the relative humidity (RH) set to 60 %
 157 and temperature to 293.15 K. The RH value considered in this study is based on previous published
 158 experimental studies performed at ~60 % in both smog chamber (Bruns et al., 2015; Ehn et al., 2014;
 159 Stirnweis et al., 2017) and OFR (Ahlberg et al., 2019). α -pinene ozonolysis runs were performed at four
 160 different temperatures: 258.15 K, 278.15 K, 303.15K and 313.15 K, respectively. SOA mass yields are
 161 expected to increase with decreasing temperature (Saathoff and Naumann, 2009). A similar temperature
 162 dependence was observed by Kristensen et al. (2017) who observed SOA mass yield from α -pinene
 163 ozonolysis at ~ 40 % and ~20 % at 258 K and 293 K respectively. Analogous to analyzing the effect of
 164 varying temperature on SOA yields, we study the variation in α -pinene ozonolysis SOA mass yields by
 165 varying the NO_x concentrations. SOA yields for α -pinene ozonolysis at high NO_x conditions should be
 166 suppressed (Ng and Chhabra, 2007), which could be due to the production of relatively, volatile organic
 167 nitrates under high NO_x conditions as compared to less volatile products during low NO_x conditions (Presto et
 168 al., 2005).

169 Furthermore, two different chemistry schemes were applied for the simulations. One scheme consisted
 170 of only the MCM chemistry mechanism and the second included the MCM+PRAM chemistry mechanism.
 171 Table 1a shows the concentrations of different BVOCs and Table 1b shows the oxidants concentrations used
 172 for the simulations.

173 **Table 1a.** Concentrations of different BVOCs

α -pinene (ppb)	β -pinene (ppb)	Isoprene (ppb)	Limonene (ppb)	β -caryophyllene (ppb)
0.5, 1.0, 5.0, 50.0, 100.0, 200.0	0.5, 1.0, 5.0, 50.0, 100.0, 200.0	5.0, 50.0, 100.0, 200.0	1.0, 5.0, 50.0, 100.0, 200.0	0.5, 1.0, 2.0, 5.0, 10.0

174

175 **Table 1b.** Concentrations of different oxidants for chamber and flow-tube runs

OH (* 10 ⁶ #/cm ³) - chamber	O ₃ (* 10 ¹¹ #/cm ³) - chamber	NO ₃ (* 10 ⁷ #/cm ³) - chamber
OH (* 10 ⁸ #/cm ³) - OFR	O ₃ (* 10 ¹³ #/cm ³) - OFR	NO ₃ (* 10 ⁹ #/cm ³) - OFR

2.0, 5.0 ,10.0, 50.0,100.0	1.0, 5.0 ,10.0, 50.0,100.0	1.0, 5.0 ,10.0, 50.0,100.0
----------------------------	----------------------------	----------------------------

176

177 **Table 1c.** NO concentrations and temperatures used for α -pinene ozonolysis

NO (ppb)	0.5 (default), 0, 0.2, 1, 2, 5
Temperature (K)	293.15 (default), 258.15, 278.15, 303.15, 313.15

178

179 **2.3 Mass Yields**

180 The SOA mass yields (Y) are determined by calculating the ratio of the amount of SOA or mass
181 concentration of organic aerosol formed (C_{OA}) to the amount of VOC (ΔVOC) reacted:

$$182 \quad Y = \frac{C_{OA}}{\Delta VOC} \quad (1)$$

183 A volatility basis set is fit to the data to obtain the volatility distribution. In this study equilibrium
184 partitioning was only assumed for deriving the volatility distribution based on the model simulations.
185 Following Donahue et al. (2006), the SOA is assumed to be in equilibrium with the gas-phase and using the
186 effective saturation concentration C_i^* spaced logarithmically. The individual product partitioning to the
187 particle phase can be estimated using

$$188 \quad E_i = \left(1 + \frac{C_i^*}{C_{OA}} \right)^{-1} \quad (2)$$

189 Where E_i is the fraction of species in the condensed particle phase. The above equation determines the
190 fraction of species in the particle phase as well as in the gas phase. For example, if we assume $C_{OA} = 10 \mu\text{g m}^{-3}$
191 a species with $C^* = 10 \mu\text{g m}^{-3}$ will partition 50 % to condensed phase and the rest 50% will reside in the gas
192 phase. The fidelity of this equilibrium partitioning enables the parameterization of product vapors in volatility
193 C^* bins that are near the C_{OA} concentrations (Henry et al., 2012).

194

195 **3. Results and Discussion**196 **3.1 BVOCs – O₃ chamber and flow-tube simulations**

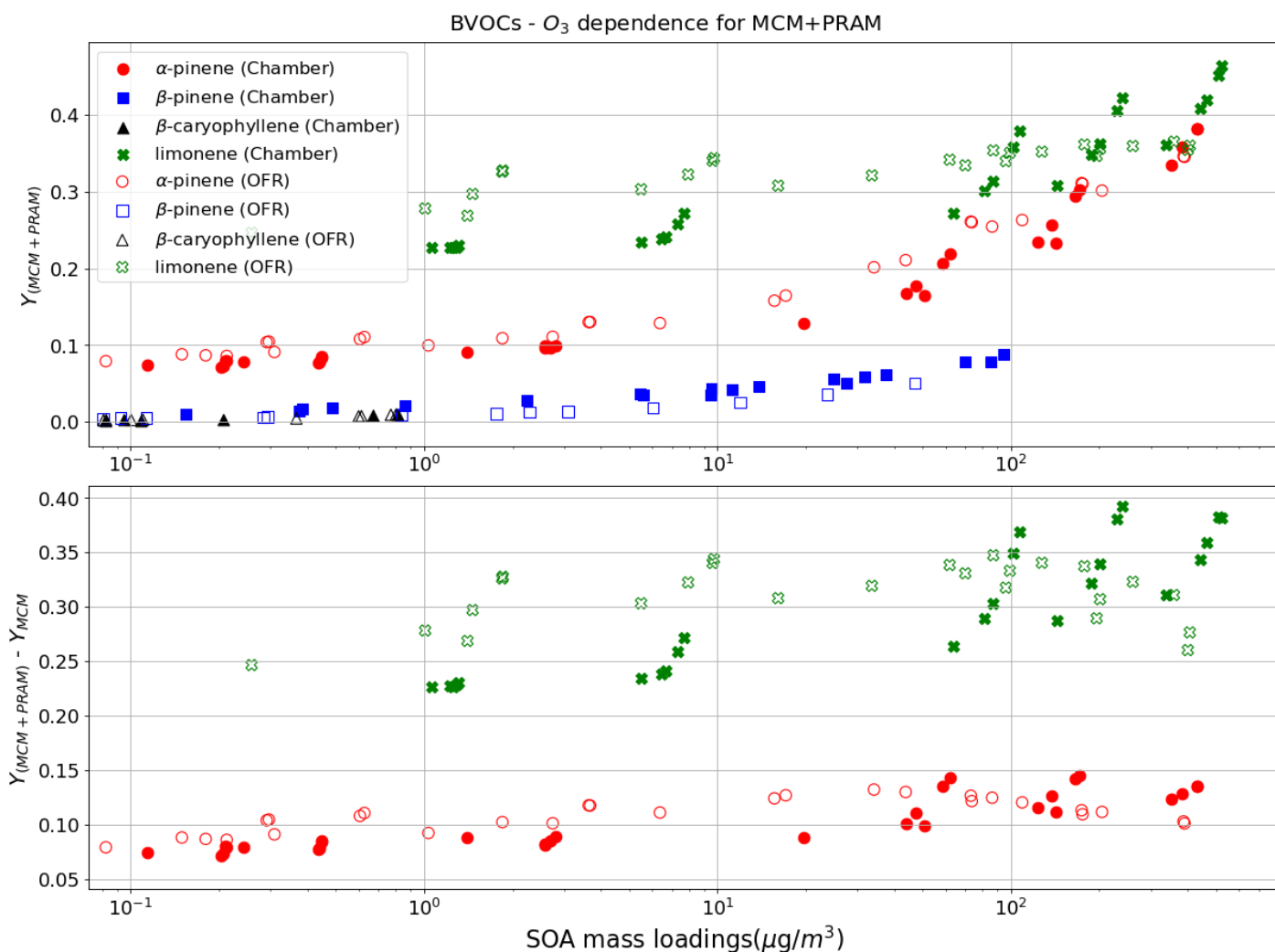
197 SOA mass yields were simulated for the oxidation of various biogenic volatile organic compounds
198 (isoprene, α -pinene, limonene and β -caryophyllene, β -pinene) by dominant atmospheric oxidants OH, O₃ and
199 NO₃. The following section examines the comparison between the yields derived using MCM+PRAM and a
200 standalone MCM for chamber and flow-tube experiments. In Fig 1. the upper panel indicates MCM+PRAM
201 contribution to SOA mass from BVOCs ozonolysis and the lower panel shows the differences between the
202 yields obtained from the MCM+PRAM ($Y_{\text{MCM+PRAM}}$) and MCM scheme ($Y_{\text{MCM+PRAM}} - Y_{\text{MCM}}$).

203 The abscissa, depicted on a log scale, considers the entire range of SOA mass loadings from 1-1150
204 $\mu\text{g}/\text{m}^3$. Each data point is representative of simulated SOA mass yields resulting from variable BVOC
205 loading. The resulting mass yields for α -pinene in the range shown in Table 2a are consistent with the yields
206 found in various smog chamber experiments. Kristensen et al. (2017) found mass yields of 0.22 and 0.21 for
207 α -pinene ozonolysis at 293 K with SOA mass loadings of 62 and 59 $\mu\text{g m}^{-3}$, respectively, while Pathak et al.
208 (2007) found similar mass yields values in the range of 0.16 – 0.21 for mass loadings between 33.7 – 50.7 $\mu\text{g m}^{-3}$.
209 m^{-3} . These values are within the range of mass yields derived using MCM+PRAM (0.15 - 0.2) while those
210 derived with only MCM severely under-predict the mass yields. The MCM+PRAM also shows better
211 agreement with experiments when estimating the lower range mass yields for SOA mass loadings of < 15 $\mu\text{g m}^{-3}$.
212 This is supported by the values obtained by Shilling et al. (2008), where the authors measured a 0.09
213 yield from α -pinene ozonolysis for SOA mass loading of 10.6 $\mu\text{g m}^{-3}$. Limonene ozonolysis mass yields using
214 MCM+PRAM in comparison to standalone MCM, are much closer to the values given by Waring (2016),
215 wherein he measured high yields of 0.26 - 1.06 for SOA loadings of 1.7 - 718.4 $\mu\text{g m}^{-3}$.

216 The formation of HOM from β -pinene ozonolysis is low (Ehn et al., 2014; Jokinen et al., 2015) and
217 hence not considered in PRAM. The peroxy radical autoxidation mechanism for β -caryophyllene ozonolysis
218 has not yet been developed and hence is not considered in PRAM. Chen et al. (2012) measured SOA particle
219 mass yield for β -caryophyllene ozonolysis in the range of 0.1- 0.2 for mass loadings $M_{\text{org}} < 10 \mu\text{g m}^{-3}$ and
220 ascertained the O₃ concentration insensitivity to the yields. Pathak et al. (2008) measured the β -pinene
221 ozonolysis mass yields in the range of 0.013- 0.081 for lower reacted concentrations (8-40 ppb) of β -pinene,
222 while Griffin (1999) measured a yield from 0.01-0.17 for reacted β -pinene in the range of 30 -180 ppb. When
223 comparing the measured mass yield values for β -caryophyllene and β -pinene ozonolysis to the modeled
224 values using the MCM scheme, it is evident that the MCM scheme drastically under-predicts the SOA mass
225 yields.

226 Today oxidation flow reactor (OFR) experiments are complementing the traditional batch mode smog
227 chamber experiments. The OFR generally exhibits lower mass yields compared to the smog chamber

228 experiments at ranges of equivalent oxidant exposure (Lambe et al., 2015). We modeled flow-tube simulation
229 after the potential aerosol mass (PAM) OFR, where the residence time is in the order of a few to several
230 minutes (Lambe et al., 2011). Our model simulations are performed with a maximum residence time of 100
231 seconds with O₃ exposures ranging from 1.0×10^{15} – 1.0×10^{17} molecules cm⁻³ s (residence time x [O₃]).
232 Kang and Root (2007) measured a value of 0.2 for ozonolysis of α -pinene for an initial precursor VOC
233 concentration of 100 ppbv, while we obtain 0.25-0.3 for the similar initial precursor concentrations. The OFR
234 yields for β -pinene are significantly lower (0.02) than the values measured by Kang and Root (2007) wherein
235 they measured a yield of 0.49 for similar initial precursor concentrations. Addition of seed particles promotes
236 condensation, leading to increased SOA yields (Lambe et al., 2015) which was confirmed by Ahlberg et al,
237 (2019). Kang and Root (2007) found that using seed particles, the yield from α -pinene ozonolysis increased
238 by a factor of ~ 1.4 which can explain our yields for α -pinene ozonolysis simulations, while the absence of a
239 PRAM for β -pinene could explain the low values from our simulation. The mass spectra plot (Figure S2)
240 shows that PRAM contributes the majority of dimers to the particle phase, while MCM dominate monomer
241 contribution. Another interesting facet of Figure S2 are the different condensing compounds in both OFR and
242 chamber simulations. The higher absolute RO₂ concentrations in the OFR simulations explain the lower
243 concentration of HOM monomers and dimers relative to the chamber simulations, i.e. the high RO₂
244 concentrations in the OFR cause termination of the peroxy radical autoxidation chain before the RO₂ become
245 highly oxygenated, thereby influencing SOA yields. Hence, this should be taken into account when using
246 yields from OFR as inputs to regional and global models.



247 **Figure 1.** The mass yields from the ozonolysis of BVOCs modelled after chamber and flow-tube settings. The figure shows a
 248 comparison of SOA mass yields obtained from simulations with MCM + PRAM and PRAM. The BVOCs are represented by α -
 249 pinene (red circles), β -pinene (blue squares), limonene (green stars) and β -caryophyllene (black triangles) with the filled and open
 250 symbols depicting the chamber and oxidation flow reactor (OFR) simulations respectively.

Table 2. Mass yields for BVOCs ozonolysis at 293 K for different range of mass loadings using a chamber[†] and OFR^{||} setup.

SOA mass loading ($\mu\text{g m}^{-3}$)	MCM + PRAM mass yields range	MCM mass yields range	BVOC	Experimental yields	References
0 - 15 [†]	0.07– 0 .08	0.00 – 0.06	α -pinene	0.09 (10.6)	Shilling et al. (2008)
16 - 60 [†]	0.12 – 0.20	0.06 – 0.11	α -pinene	0.16 - 0.21	Pathak et al. (2007)

61 – 200 [†]	0.22 – 0.30	0.12 – 0.15	α -pinene	0.22 (62)	Kristensen et al. (2017)
1.1– 550 [†]	0.24 -0.48	0.007-0.06	limonene	0.26-1.06	Waring (2016)
0-100	0.07-0.25	0-0.13	α -pinene	0.2	Kang and Root (2007)

251

252 3.2 BVOCs – OH chamber and flow-tube simulations

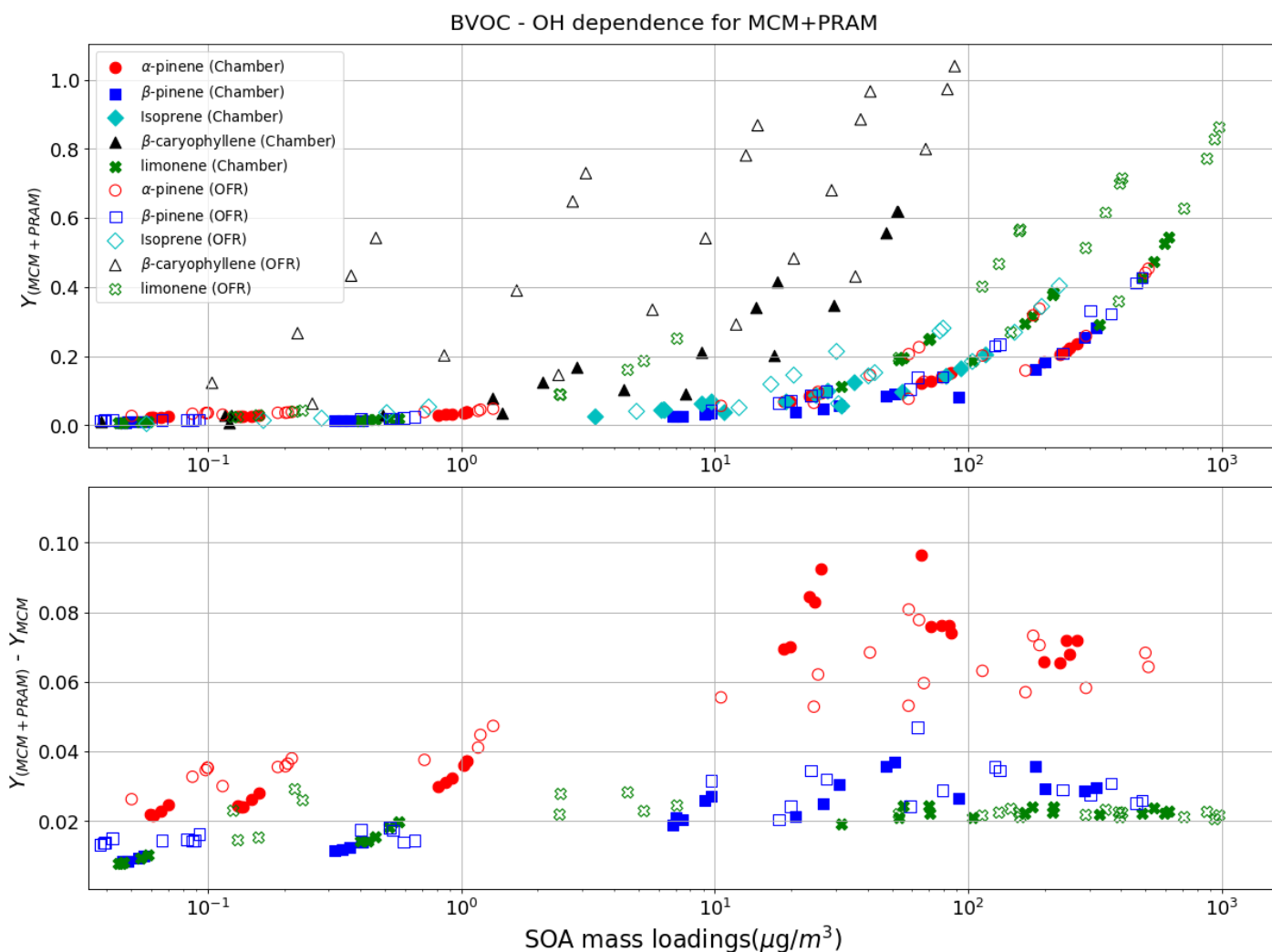
253 The ΔY in the lower panel of Figure 2 for limonene, β -pinene and α -pinene resulting from the fact that
254 PRAM considers peroxy radical autoxidation product formation from OH oxidation of these BVOC's. The
255 results for SOA mass yields of OH oxidation of α -pinene using MCM+PRAM is close to the measured values
256 (Kristensen et al., 2017), while using only MCM under-predicts the mass yields. Similarly, the current lack of
257 peroxy radical autoxidation product mechanism for β -caryophyllene and isoprene result in $\Delta Y = 0$ values for
258 PRAM. The maximum SOA mass yield for OH oxidation of α -pinene is lower than the yield from ozonolysis
259 which is suspected to arise due to the formation of more volatile oxidation products produced during OH
260 oxidation (Bonn and Moortgat, 2002; Kristensen et al., 2014). For β -caryophyllene, Griffin (1999) measured
261 SOA mass yields in the range of 0.37 – 0.79 for mass loadings of 17 - 82 $\mu\text{g m}^{-3}$ while Tasoglou and Pandis
262 (2015) measured yields around 0.2 for photo-oxidation at low NO_x conditions for loadings of 10 $\mu\text{g m}^{-3}$.
263 These values are in good agreement with our results which show a similar yield range of 0.3 – 0.7 for
264 loadings between 20 - 100 $\mu\text{g m}^{-3}$ and 0.21 for loading of 10 $\mu\text{g m}^{-3}$. Currently there are no experiments
265 providing HOM yields from experiments of OH oxidation of β -caryophyllene, and hence, not included in
266 PRAM. The simulation results for yields from OH oxidation of β -caryophyllene, indicate that the MCM
267 scheme is able to reproduce the experimental values. The mass yields derived from OH oxidation of isoprene
268 vary from 0.01 - 0.31 covering a range of mass loadings from 0.003 - 132 $\mu\text{g m}^{-3}$. At low mass loadings < 10
269 $\mu\text{g m}^{-3}$ the maximum yield obtained is ~ 0.06 , which is a factor of 2 greater than the experimental results
270 obtained by Lee et al. (2006) and Kroll et al. (2005), where they measured yields of 0.02 and 0.01 – 0.03
271 respectively. Liu et al. (2016) measured higher mass yields (> 0.1) for similar loadings with a maximum
272 upper limit yield of 0.15 for 22 $\mu\text{g m}^{-3}$, while our results under-predict the yields (~ 0.10) for similar
273 loadings. The OH oxidation of β -pinene and limonene results in a maximum yield of 0.28 for high mass
274 loading of 319 $\mu\text{g m}^{-3}$ and 0.56 for loadings of 630 $\mu\text{g m}^{-3}$ respectively. These values are similar to the
275 measurements obtained by Lee et al. (2006) wherein they measured a yield of 0.31 for β -pinene SOA mass
276 loadings of 293 $\mu\text{g m}^{-3}$ and 0.58 for limonene SOA mass loadings of 394 $\mu\text{g m}^{-3}$. Yields for limonene SOA
277 mass loadings of 350 $\mu\text{g m}^{-3}$ are around 0.31 which is lower than the experimental values, measured by Lee et

278 al. (2006). The β -pinene SOA yields are comparatively well represented by MCM+PRAM in comparison to
 279 the standalone MCM. On the other hand, the limonene mass yields are under-predicted by MCM+PRAM.

280 The OFR simulations results for the OH oxidation of BVOCs with an equivalent exposure range from
 281 $2.0 \times 10^{10} - 2.0 \times 10^{12}$ molecules cm^{-3} s, is shown in Fig. 2. Friedman and Farmer (2018) found mass yields
 282 of $7 \times 10^{-4} - 0.086$ for α -pinene (ammonium sulfate seeded experiment), 0 - 0.12 for β -pinene (no seed
 283 particles) and 0.0017 - 0.026 for limonene (no seed particles), by varying the OH exposures between $4.7 \times$
 284 $10^{10} - 7.4 \times 10^{11}$ molecules cm^{-3} s. Our simulated yields for OH oxidation of α -pinene ($\sim 0.05 - 0.31$), β -
 285 pinene ($\sim 0.019 - 0.2$) and limonene suggest higher mass yields at both measured lower and higher values of
 286 values of OH exposures and monoterpene concentrations ($\sim 12 - 270$ ppb). In contrast to the experiments,
 287 every simulation contained higher particle surface area, which could explain the higher simulated mass yields
 288 for the compounds.

Table 3. Mass yields for OH oxidation of BVOCs at 293 K for different range of mass loadings using a chamber[†] and OFR^{||} setup.

SOA mass loading ($\mu\text{g m}^{-3}$)	MCM + PRAM mass yields	MCM mass yields	BVOC	Experimental yields	References
320 [†]	0.28	0.25	β -pinene	0.31	Lee et al. (2006)
350 [†]	0.31	0.06 – 0.11	limonene	0.58	Lee et al. (2006)
0-300	0.05 – 0.31	0. – 0.2	α -pinene	$7 \times 10^{-4} - 0.086$	Friedman and Farmer (2018)
0-300	0.019-0.2	0-0.13	β -pinene	0 - 0.12	Friedman and Farmer (2018)

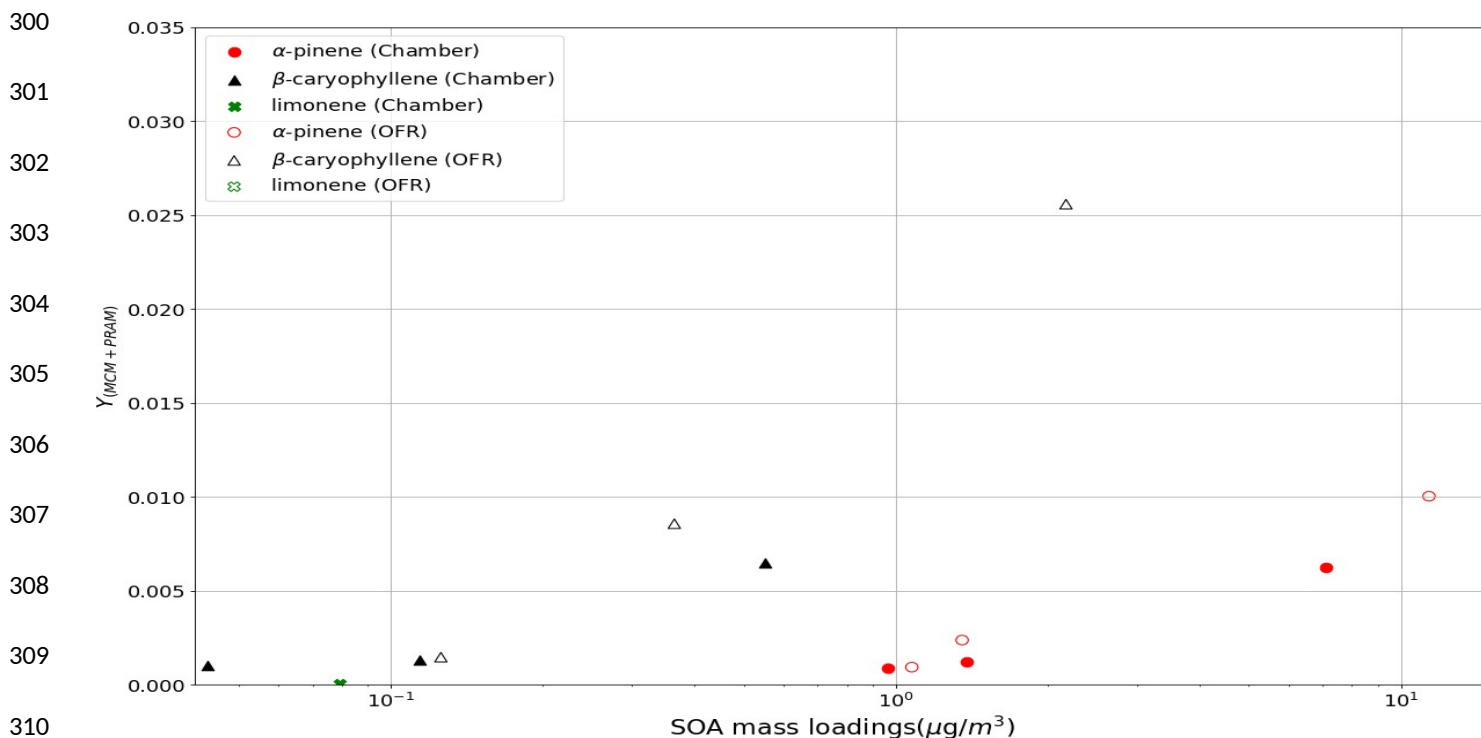


289 **Figure 2.** The mass yields from OH oxidation of BVOCs modeled after chamber and flow-tube settings. The figure shows a
 290 comparison of SOA mass yields obtained from application of MCM+PRAM and only MCM. The color scheme is the same as in
 291 figure 1. Additionally, isoprene has been included as it reacts with OH and produces considerable SOA yields.

292 BVOC – NO₃ chamber and OFR simulations

293 The yields obtained for oxidation of α -pinene (0.002-0.007) by NO₃ are low in comparison to those
 294 obtained by Nah et al. (2016), where they measured a yield of 0.036. Measured mass yields for limonene
 295 oxidation by NO₃ resulting in mass yields between 0.25-0.4 (Fry et al., 2011), whereas we obtain negligible
 296 (~0.0003) mass yields for the same. Due to limited experimental constraints, PRAM presently does not
 297 consider autoxidation of RO₂ formed from NO₃ oxidation of VOCs, which could explain the huge discrepancy
 298 between the measured and simulated mass yields.

299

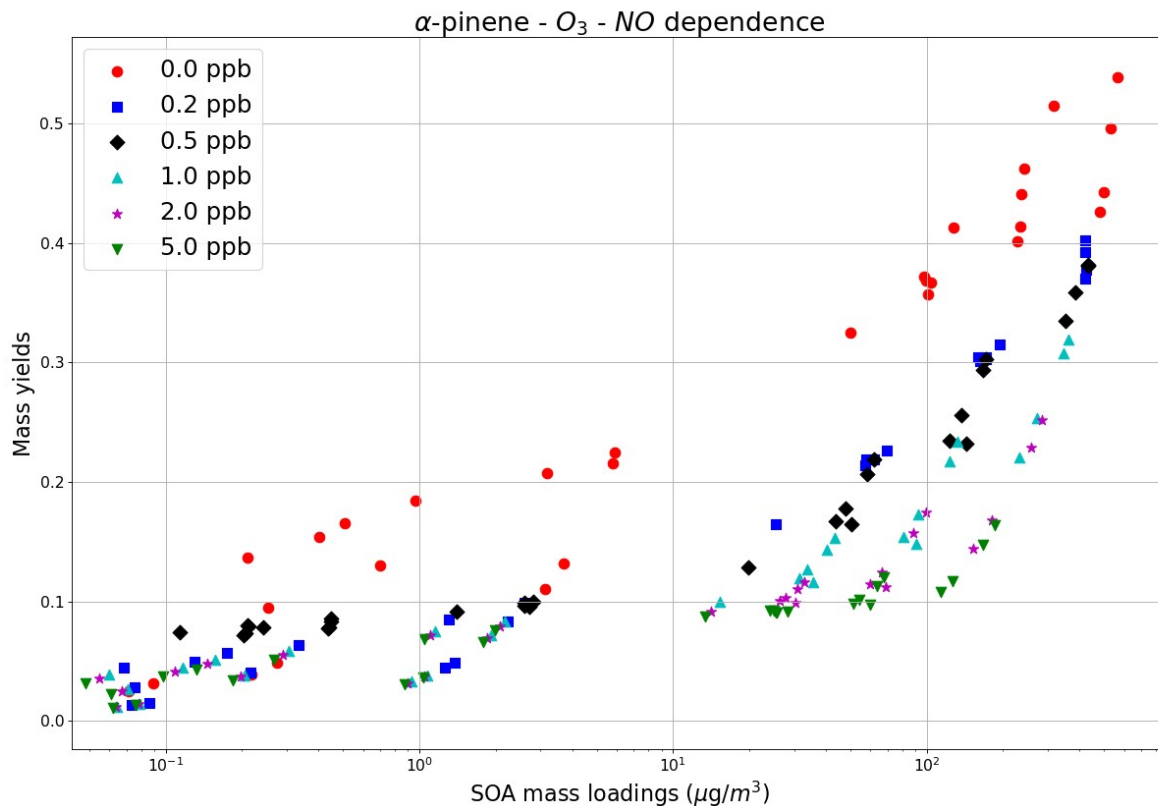
BVOC - NO_3 dependence for MCM+PRAM

310

311 **Figure 3.** The mass yields from NO_3 oxidation of BVOCs modeled after chamber and flow-tube settings. The figure shows a
 312 comparison of SOA mass yields obtained from application of MCM+PRAM. Appreciable mass yields were only obtained for α -
 313 pinene, limonene and β -caryophyllene.

314 3.3 NO_x dependence

315 Organic oxidation mechanisms are sensitive to NO_x concentrations as they change the fate to RO_2
 316 radical formed, thereby impacting the distribution of reaction products and aerosol formation (Presto et al.,
 317 2005; Zhao et al., 2018). We modeled the SOA mass yields for α -pinene - O_3 setup with varying NO_x
 318 concentrations (NO was varied whereas NO_2 was kept constant for all the runs), for initial α -pinene mixing
 319 ratios in the range 0.5 - 200 ppb (Fig. 4). A maximum SOA yield value of 0.55 is obtained for a combination
 320 of the lowest value of NO (0 ppb, red circles). As the NO concentrations increase from 0.2 ppb (blue squares)
 321 to 5 ppb (green inverted triangles) the yields begin to decrease, and this pattern is observable and valid for all
 322 concentration ranges of reacted precursor VOC. The NO_x dependence of α -pinene ozonolysis is consistent
 323 with the findings of Draper et al. (2015) and Presto et al. (2005) wherein they observed a trend of decreasing
 324 SOA mass yields for α -pinene ozonolysis with increasing NO_x concentrations. NO_x concentrations alter the
 325 HO_2/RO_2 ratio thereby impacting competing peroxy radical (RO_2) reaction pathways (Presto et al., 2005;
 326 Sarrafzadeh et al., 2016).

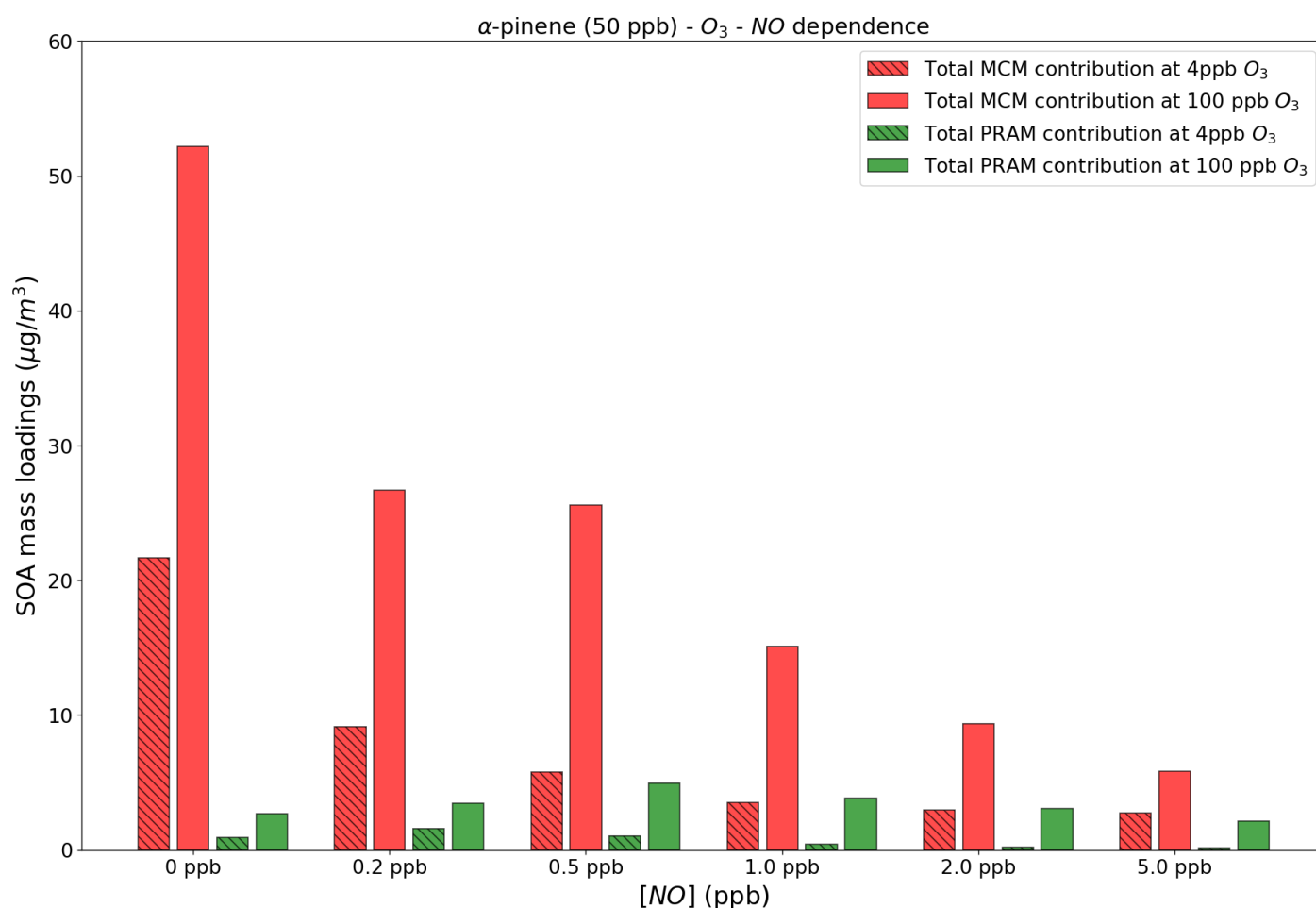


327 **Figure 4.** The SOA mass yields from O₃ oxidation of α-pinene modeled for different NO concentrations with the chamber setup.
 328 The model runs were performed using MCM+PRAM.

329 At low NO_x concentrations RO₂ radicals undergo rapid autoxidation until they react with HO₂ or RO₂
 330 resulting in production of low volatility hydro-peroxide products (Sarrafzadeh et al., 2016), closed shell
 331 monomers or dimers (Ehn et al., 201; Roldin et al., 2019), which increase SOA mass. This contrasts with high
 332 NO_x conditions where the RO₂+NO reactions dominate over reactions with HO₂ or RO₂, resulting in the
 333 formation of more volatile products such as aldehydes, ketones and organonitrates (Presto et al., 2005;
 334 Sarrafzadeh et al., 2016), and likely suppressing the autoxidation process leading to a decrease in SOA mass
 335 loadings (Ehn et al., 2014).

336 Figure 5 shows the absolute contributions to SOA mass loadings by PRAM and MCM compounds at
 337 two different O₃ concentrations of 4 and 100 ppb and varying NO concentrations. The figure shows that with
 338 an increase in NO concentrations the contribution of PRAM compounds to the particle phase decreases at
 339 both 4 and 100 ppb of O₃ concentrations. In PRAM the RO₂ + NO reaction leads either to the formation of
 340 organonitrate HOM, closed shell monomers with carbonyl group or fragmentation products with higher
 341 volatility (Roldin et al., 2019). HOM Dimer formation is suppressed with increasing NO concentrations in

342 PRAM (Roldin et al., 2019) which explains the lower contribution by PRAM compounds to SOA mass
 343 loadings with increasing NO. The PRAM contribution increases at low NO (<1 ppb) and then decreases
 344 thereafter. At low NO concentrations (<1ppb), first generation RO₂ are capable of undergoing autoxidation
 345 forming highly oxygenated RO₂ which subsequently reacts with NO forming organic nitrates (Ehn et al.,
 346 2014). As NO concentrations exceed 1ppb the first generation RO₂ is scavenged by NO thereby reducing the
 347 concentration of organonitrate HOM (Ehn et al., 2014), possibly affecting SOA yields. The MCM
 348 contribution also decreases with increasing NO concentrations mostly due to the formation more volatile
 349 organonitrates (Jenkin et al., 2019) .



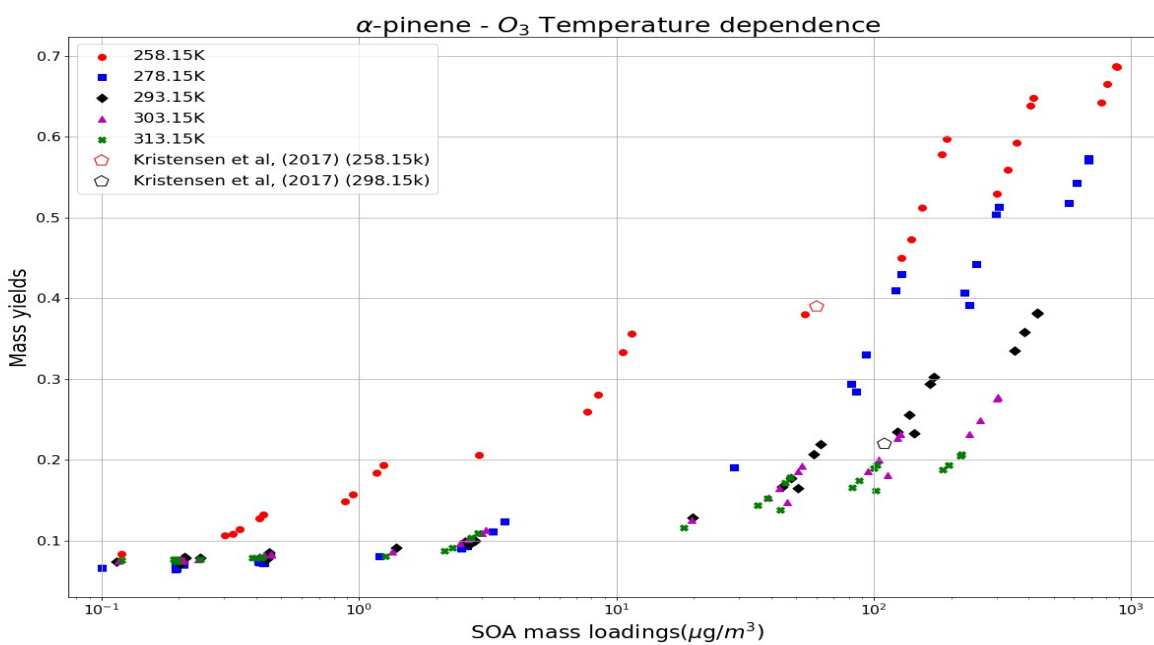
350 **Figure 5.** Contribution to the SOA mass loadings by total PRAM and MCM compounds at different NO_x levels and O₃
 351 concentrations. For comparison we use 4 ppb and 100 ppb O₃ concentrations, respectively, at 50 ppb α -pinene.

352 3.4 Temperature dependence

353 The formation of SOA from α -pinene ozonolysis in the temperature range of 258.15 - 313.15 K was
 354 investigated in this study using MCM+PRAM. Strong dependence of SOA mass yield on temperature was
 355 reported by Saathoff and Naumann, (2009) wherein they measured the decreasing mass yields from 0.42 at

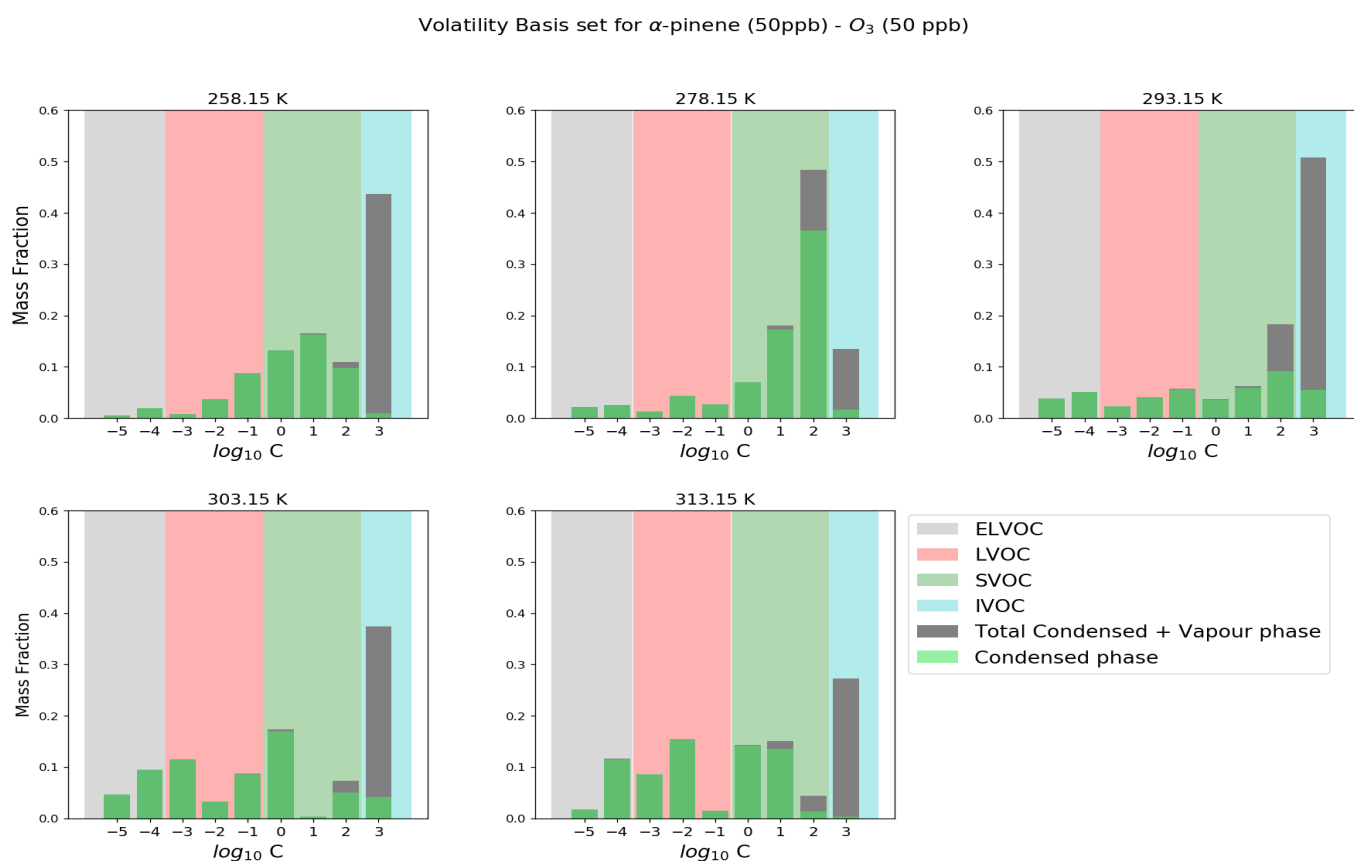
356 273.15 K to 0.09 to 313.15 K for SOA loadings of 53 and 92 $\mu\text{g m}^{-3}$ respectively. Our results in Figure 6
 357 show increasing SOA mass yields for α -pinene ozonolysis with decreasing temperature, which is attributed to
 358 the augmented condensation of oxidation products termed as semi volatile organic compounds (SVOC)
 359 (Kristensen et al., 2017) at lower temperatures.

360 For α -pinene maximum mass loading $< 150 \mu\text{g m}^{-3}$ the mass yields reach a maximum value of 0.38 at
 361 temperatures as low as 258.15 K and decreases to 0.27 for a temperature of 293.15 K to 0.1 for the
 362 temperature of 313.15 K. These yields are comparable to the results obtained by Kristensen et al.
 363 (2017) where they measured yields of 0.39 for 258.15 K and 0.22 for 293.15 K for mass loading $< 150 \mu\text{g m}^{-3}$.
 364 The results show a weak dependence of SOA mass yields on temperatures in the range of 278.15 K - 313.15
 365 K at low SOA mass loadings but become more pronounced as the mass loadings increase. At the lowest
 366 temperature of 258.15 K the mass yields are higher in comparison to other temperatures regardless the mass
 367 loadings. These results are in good agreement with the findings by Pathak et al. (2007) where they found a
 368 strong temperature dependence of SOA mass yields at lower temperature ($0 - 15^\circ \text{C}$), which decreases as the
 369 temperature increases. Furthermore, similar to the measurements made by Pathak et al. (2007), our
 370 simulations were able to reproduce the experimental findings that show no appreciable differences in the SOA
 371 mass yields for loadings below $1 \mu\text{g m}^{-3}$ (initial mixing ratio of 1 ppb) for temperatures $> 273.15 \text{ K}$.



372 **Figure 6.** Temperature dependence of SOA mass yields at different temperatures using the MCM+PRAM. The open pentagons
 373 represent measurement data from Kristensen et al. (2017) at 258.15 K and 298.15 K.

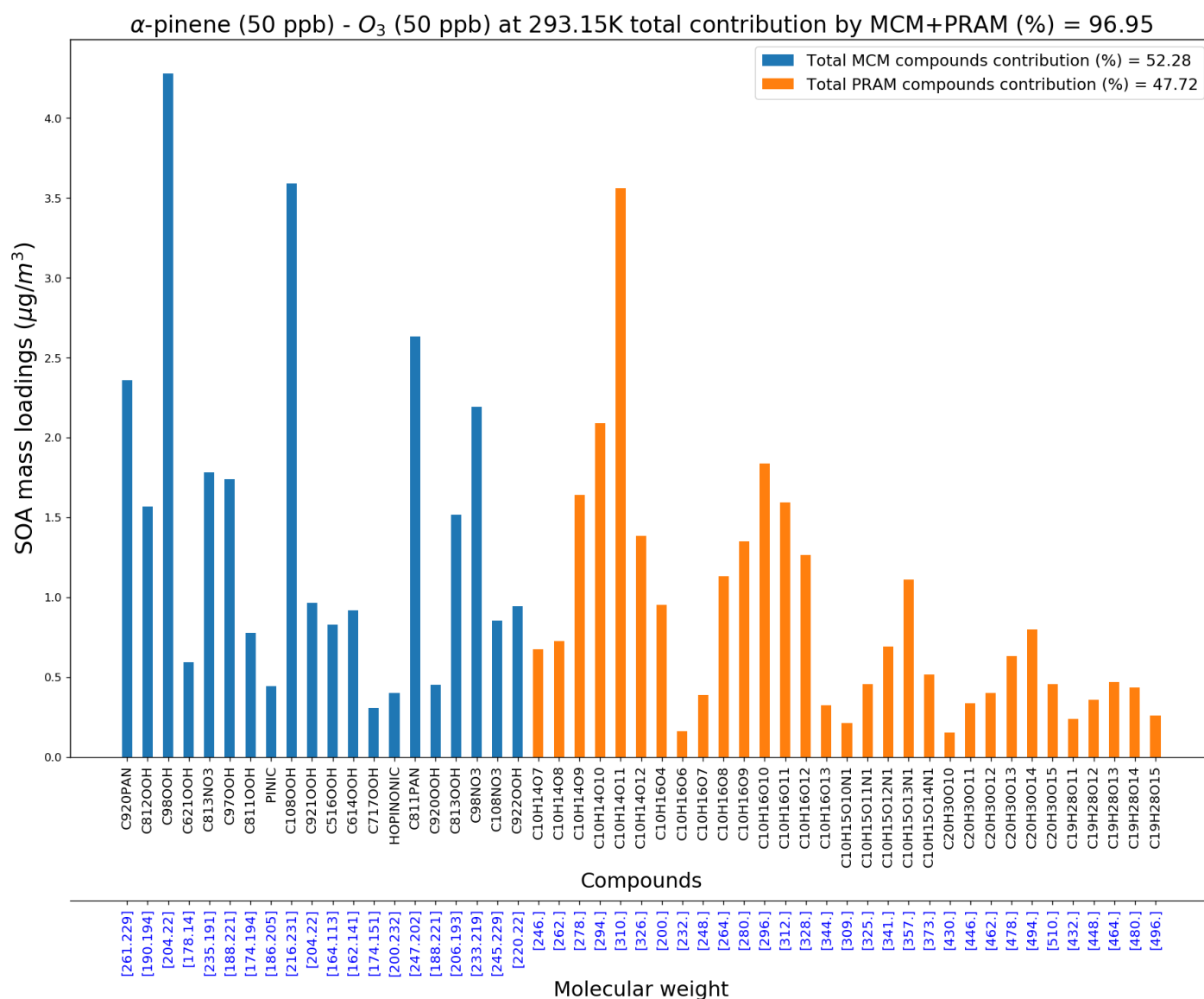
374 Figure 7 shows the volatility distribution of α -pinene ozonolysis derived SOA at different
 375 temperatures. The saturation vapor pressure limits for defining extremely low volatility (ELVOCs - grey
 376 shaded), low volatility (LVOCs - red shaded), semi volatile (SVOCs - green shaded) and intermediate
 377 volatility (IVOCs - cyan shaded) organic compounds used in the Volatility basis set (VBS) are set according
 378 to the values suggested in Donahue et al. (2012). In this work, we categorize compounds (ELVOCs, LVOCs,
 379 SVOCs and IVOCs) based on effective saturation vapor pressures (C^*) in the range of $\{10^{-5}$ to $10^3\}$ $\mu\text{g m}^{-3}$
 380 and temperature of 298 K (Donahue et al., 2009). At the lowest temperature of 258.15 K, the SVOCs
 381 contribution to the particle phase is dominant in comparison to LVOCs and ELVOCs, a trend which is
 382 subsequently reversed as the temperatures are increased. At 293.15 K a majority of SVOCs and IVOCs are in
 383 the gas phase while the contribution of LVOCs and ELVOCs to particle phases increases. These results are in
 384 good agreement with observations made by Kristensen et al. (2017) wherein they observed an increasing
 385 contribution of SVOCs at sub-zero temperatures of 258.15 K, which decrease the fraction of SOA formed
 386 from ELVOCs. Again, it should be noted that the temperature dependence of peroxy radical autoxidation
 387 product formation still needs further validation based on recent experiments (e.g. Quéléver et al., 2018).
 388



389 **Figure 7.** Modeled volatility distribution of SOA at different temperatures. The volatility bins span a range of effective saturation
 390 vapor pressures $C = C^* = \{10^{-5}$ to $10^3\}$ $\mu\text{g m}^{-3}$. The VBS distribution is based on a reference temperature of 298 K.

391 **3.5 Composition**

392 MCM+PRAM can be used to narrow down and compile a list of compounds playing a pivotal role in
 393 contributing to SOA mass loadings and, also compare the relative importance of implementing PRAM
 394 alongside the MCM. Figure 8 shows the most important compounds from both the MCM and PRAM that
 395 condense on the seed particles and have a dominant contribution (>95%) to the α -pinene ozonolysis SOA
 396 mass loading at 293 K.



397 **Figure 8.** MCM and PRAM Compounds contributing to > 95 % of SOA mass at 293 K and 50ppb O_3 and α -pinene concentrations.

398 At 293 K (Figure 8) the listed compounds (MCM+PRAM) contribute ~97 % to the SOA mass loading with
 399 PRAM compounds contributing to ~48 % (of 97 %) in comparison to MCM compounds which contribute ~52
 400 % (of 97%). On lowering the temperature to 258K the relative contributions of PRAM drop to 15 % (of ~98

401 %), while MCM dominates by contributing ~85 % (of ~98 %) respectively (Figure S3a). The contribution of
402 PRAM increases to ~64 % (of ~97 %) and MCM contribution drops to 36 % (of ~97 %) at 313 K (Figure
403 S3b). These results reflect the importance of PRAM as its contribution plays an increasingly dominant role
404 with increasing temperatures and highlights the crucial few compounds that contribute to maximum SOA
405 mass loadings for α -pinene ozonolysis. The list of abundant compounds which together add up to contribute
406 more than 95 % of SOA mass loadings at 258 K, 293 K and 313 K are presented in the supplement Table 1s
407 (a, b & c). At 258 K MCM compounds namely pinonic acid ($C_{10}H_{16}O_3$, 4.4 %), C920PAN ($C_{10}H_{15}NO_7$, 9.3
408 %), C108NO3 ($C_{10}H_{15}NO_6$, 8.9 %), C811PAN ($C_9H_{13}NO_7$, 10.1 %), C717NO3 ($C_7H_9NO_6$, 11.3 %) contribute
409 significantly to the total SOA mass loadings while PRAM compounds such as $C_{10}H_{14}O_7$ (0.88 %), $C_{10}H_{16}O_4$
410 (1.3 %), $C_{10}H_{16}O_6$ (1.13 %) contribute significantly less. An increase in temperature to 293 K results in an
411 overall increase in contribution by PRAM compounds, with $C_{10}H_{14}O_{10}$ (3.6 %), $C_{10}H_{14}O_{11}$ (6.2 %), $C_{10}H_{16}O_{10}$
412 (3.2 %) playing an important role in contributing to the SOA mass loadings. This trend of relative increase in
413 the contribution by PRAM compounds over MCM compounds to SOA mass loadings is also evident as the
414 temperatures are further increased to 313 K, where the PRAM compounds $C_{10}H_{14}O_{11}$ (18.3 %), $C_{10}H_{14}O_{12}$ (6
415 %) and $C_{10}H_{16}O_{12}$ (6.6 %) play a dominant role in increasing SOA mass loadings.

416 **Conclusions**

417 We simulated SOA mass yields derived from the oxidation of various BVOCs (isoprene, α -pinene, β -
418 pinene, limonene and β -caryophyllene), by the oxidants O_3 , OH and NO_3 using the zero-dimensional model
419 MALTE-Box. The gas phase chemistry was simulated using the MCM in conjunction with PRAM. The aim
420 was to verify the efficacy of MCM+PRAM in simulating the SOA mass yields. Additional simulations were
421 performed to test the MCM+PRAM under varying temperature and NO concentrations. A few important
422 compounds playing a major role in increasing the SOA mass yields for α -pinene ozonolysis at different
423 temperatures are also highlighted.

424 The simulations were designed to resemble ideal smog chambers experiments and experiments in
425 oxidative flow reactors (OFR). No interactions between the gas phase and chamber walls were considered
426 during the simulations. For the smog chamber setting, the standalone MCM generally under-predicts the mass
427 yields obtained by the ozonolysis and OH oxidation of BVOCs. In contrast, the yields derived using
428 MCM+PRAM for the smog chamber setup is in good agreement with the experimental results. For an
429 idealized OFR setup, MCM+PRAM over-predicts the yields in case of ozonolysis and OH oxidation of
430 BVOCs, while again the MCM under-predicts the SOA yields. This over prediction in mass yields for the
431 OFR simulation was a result of higher CS used in the OFR. The relative contribution of HOM monomers and

432 dimers to the particle phase in OFR simulations is low when compared to the chamber simulations. This is
433 due to higher RO₂ concentrations in OFR leading to termination of peroxy radical autoxidation, thereby
434 affecting SOA yields. This needs to be considered when applying yields based on OFR simulations in
435 regional or global chemical transport models

436 The BVOCs included in this study do not produce appreciable SOA mass yields when oxidized with
437 NO₃, as PRAM currently does not consider autoxidation of RO₂ formed from NO₃ oxidation of VOCs. This
438 underlines the need for developing a NO₃ oxidation scheme which can better constrain and predict SOA mass
439 yields. In accordance to the previous studies, the simulated SOA yields tend to decrease at higher
440 temperatures. The PRAM contribution to mass yields at low temperatures (258.15 K) is ~14 %, which is
441 substantially lower in comparison to MCM (~86 %). As the temperature is increased to 313.15 K, the
442 contribution of PRAM to SOA mass yields begins to dominate over MCM. This most likely is due to MCM
443 containing more SVOCs (compounds classified as SVOCs at 298 K), which show stronger contribution to
444 particle phase at lower temperatures, due to decrease in saturation vapor pressures with temperature. It should
445 be noted that the present temperature dependency of mass yields using PRAM are a first, and currently the
446 best estimate in understanding the influence of temperature on the peroxy radical autoxidation formation. The
447 simulated SOA yields with varying NO concentrations agree well with experimental results, i.e. SOA yields
448 decrease with increasing NO concentrations due to the formation of more volatile compounds such as
449 organonitrates and ketones.

450 Using PRAM in addition to MCM has paved way to bridge the gap in understanding the role and
451 contribution of peroxy radical autoxidation to SOA formation. The variation of SOA yields for temperature
452 and NO concentrations, indicates the limitations of global and regional models in predicting e.g. cloud
453 condensation nuclei (CCN) effects using fixed SOA yields. The good agreement of modeled and experimental
454 yields from smog chambers, respectively, could further help us parameterize the SOA yields, that could be
455 applied at a global and regional model scale, to more accurately predict the direct and indirect impact of
456 aerosol particles on e.g. radiation balance by aerosol scattering/absorption and CCN concentrations.

457 **Author Contributions**

458 CX and MB served as the chief authors and editors of the paper. CX was performing the model simulations.
459 The study was designed by CX, MB and PR. All other co-authors contributed to the analysis and writing of
460 the paper.

462 **Acknowledgements**

463 The presented research has been funded by the Academy of Finland (Center of Excellence in Atmospheric
464 Sciences) grant no. 4100104 and the Swedish Research Council FORMAS, project no. 2018-01745.

465 **References**

- 466 Ahlberg, E., Eriksson, A., Brune, W. H., Roldin, P. and Svenningsson, B.: Effect of salt seed particle surface
467 area, composition and phase on secondary organic aerosol mass yields in oxidation flow reactors, *Atmos.*
468 *Chem. Phys.*, 19(4), 2701–2712, doi:10.5194/acp-19-2701-2019, 2019.
- 469 Berndt, T., Richters, S., Jokinen, T., Hyttinen, N., Kurtén, T., Otkjær, R. V., Kjaergaard, H. G., Stratmann, F.,
470 Herrmann, H., Sipilä, M., Kulmala, M. and Ehn, M.: Hydroxyl radical-induced formation of highly oxidized
471 organic compounds, *Nat. Commun.*, 7(May), doi:10.1038/ncomms13677, 2016.
- 472 Bianchi, F., Garmash, O., He, X., Yan, C., Iyer, S., Rosendahl, I., Xu, Z., Rissanen, M. P., Riva, M., Taipale,
473 R., Sarnela, N., Petäjä, T., Worsnop, D. R., Kulmala, M., Ehn, M. and Junninen, H.: The role of highly
474 oxygenated molecules (HOMs) in determining the composition of ambient ions in the boreal forest, *Atmos.*
475 *Chem. Phys.*, 17(22), 13819–13831, doi:10.5194/acp-17-13819-2017, 2017.
- 476 Bianchi, F., Kurtén, T., Riva, M., Mohr, C., Rissanen, M. P., Roldin, P., Berndt, T., Crouse, J. D.,
477 Wennberg, P. O., Mentel, T. F., Wildt, J., Junninen, H., Jokinen, T., Kulmala, M., Worsnop, D. R., Thornton,
478 J. A., Donahue, N., Kjaergaard, H. G. and Ehn, M.: Highly Oxygenated Organic Molecules (HOM) from Gas-
479 Phase Autoxidation Involving Peroxy Radicals: A Key Contributor to Atmospheric Aerosol, *Chem. Rev.*,
480 doi:10.1021/acs.chemrev.8b00395, 2019.
- 481 Bonn, B. and Moortgat, G. K.: New particle formation during α - and β -pinene oxidation by O₃, OH and NO₃,
482 and the influence of water vapour: Particle size distribution studies, *Atmos. Chem. Phys.*, 2(3), 183–196,
483 doi:10.5194/acp-2-183-2002, 2002.
- 484 Boy, M., Hellmuth, O., Korhonen, H., Nilsson, E. D., Revelle, D., Turnipseed, A., Arnold, F. and Kulmala,
485 M.: MALTE - Model to predict new aerosol formation in the lower troposphere, *Atmos. Chem. Phys.*, 6(12),
486 4499–4517, doi:10.5194/acp-6-4499-2006, 2006.
- 487 Bruns, E. A., El Haddad, I., Keller, A., Klein, F., Kumar, N. K., Pieber, S. M., Corbin, J. C., Slowik, J. G.,
488 Brune, W. H., Baltensperger, U. and Prévôt, A. S. H.: Inter-comparison of laboratory smog chamber and flow
489 reactor systems on organic aerosol yield and composition, *Atmos. Meas. Tech.*, 8(6), 2315–2332,
490 doi:10.5194/amt-8-2315-2015, 2015.
- 491
- 492 Chen, Q., Li, Y. L., McKinney, K. A., Kuwata, M. and Martin, S. T.: Particle mass yield from β -
493 caryophyllene ozonolysis, *Atmos. Chem. Phys.*, 12(7), 3165–3179, doi:10.5194/acp-12-3165-2012, 2012.
- 494 Crouse, J. D. and Nielsen, L. B.: Autoxidation of Organic Compounds in the Atmosphere, *J. Phys. Chem.*
495 *Lett.*, 24(4), 3513–3520, doi:10.1021/jz4019207, 2013.
- 496 Damian, V., Sandu, A., Damian, M., Potra, F. and Carmichael, G. R.: The kinetic preprocessor KPP - A
497 software environment for solving chemical kinetics, *Comput. Chem. Eng.*, 26(11), 1567–1579,
498 doi:10.1016/S0098-1354(02)00128-X, 2002.
- 499 Donahue, N. M., Robinson, A. L., Stanier, C. O. and Pandis, S. N.: Coupled Partitioning, Dilution, and
500 Chemical Aging of Semivolatile Organics, *Environ. Sci. Technol.*, 40(8), 2635–2643, doi:10.1021/es052297c,
501 2006.

- 502 Donahue, N. M., Robinson, A. L. and Pandis, S. N.: Atmospheric organic particulate matter: From smoke to
503 secondary organic aerosol, *Atmos. Environ.*, 43(1), 94–106,
504 doi:<https://doi.org/10.1016/j.atmosenv.2008.09.055>, 2009.
- 505 Donahue, N. M., Kroll, J. H., Pandis, S. N. and Robinson, A. L.: A two-dimensional volatility basis set-Part 2:
506 Diagnostics of organic-aerosol evolution, *Atmos. Chem. Phys.*, 12(2), 615–634, doi:10.5194/acp-12-615-
507 2012, 2012.
- 508 Draper, D. C., Farmer, D. K., Desyaterik, Y. and Fry, J. L.: A qualitative comparison of secondary organic
509 aerosol yields and composition from ozonolysis of monoterpenes at varying concentrations of NO₂, *Atmos.*
510 *Chem. Phys.*, 15(21), 12267–12281, doi:10.5194/acp-15-12267-2015, 2015.
- 511 Ehn, M., Thornton, J. A., Kleist, E., Sipilä, M., Junninen, H., Pullinen, I., Springer, M., Rubach, F., Tillmann,
512 R., Lee, B., Lopez-Hilfiker, F., Andres, S., Acir, I. H., Rissanen, M., Jokinen, T., Schobesberger, S.,
513 Kangasluoma, J., Kontkanen, J., Nieminen, T., Kurtén, T., Nielsen, L. B., Jørgensen, S., Kjaergaard, H. G.,
514 Canagaratna, M., Maso, M. D., Berndt, T., Petäjä, T., Wahner, A., Kerminen, V. M., Kulmala, M., Worsnop,
515 D. R., Wildt, J. and Mentel, T. F.: A large source of low-volatility secondary organic aerosol, *Nature*,
516 506(7489), 476–479, doi:10.1038/nature13032, 2014.
- 517 Friedman, B. and Farmer, D. K.: SOA and gas phase organic acid yields from the sequential photooxidation
518 of seven monoterpenes, *Atmos. Environ.*, 187(January), 335–345, doi:10.1016/j.atmosenv.2018.06.003, 2018.
- 519 Fry, J. L., Kiendler-Scharr, A., Rollins, A. W., Brauers, T., Brown, S. S., Dorn, H. P., Dubé, W. P., Fuchs, H.,
520 Mensah, A., Rohrer, F., Tillmann, R., Wahner, A., Wooldridge, P. J. and Cohen, R. C.: SOA from limonene:
521 Role of NO₃ in its generation and degradation, *Atmos. Chem. Phys.*, 11(8), 3879–3894, doi:10.5194/acp-11-
522 3879-2011, 2011.
- 523 Griffin, R. J.: Organic aerosol formation from the oxidation of biogenic hydrocarbons, , 104(D3), 3555–3567,
524 1999.
- 525 Guenther, A., Baugh, B., Brasseur, G., Greenberg, J., Harley, P., Klinger, L., Serca, D., and Vierling, L.:
526 Isoprene emission estimates and uncertainties for the Central African EXPRESSO study domain, *J. Geophys.*
527 *Res. Atmos.*, 104(D23), 30625–30639, doi:10.1029/1999JD900391, 1999.
- 528 Guenther, A., Nicholas Hewitt, C., David, E., Fall, R., Chris, G., Tom, G., Peter, H., Klinger, L., Manuel, L.,
529 Mckay, W. A., Tom, P., Scholes, B., Steinbrecher, R., Tallamraju, R., Taylor, J. and Zimmerman, P.: A
530 global model of natural volatile organic compound emissions s Raja the balance Triangle changes in the
531 atmospheric accumulation rates of greenhouse Triangle Several inventories of natural and Exposure
532 Assessment global scales have been two classes Fores, *J. Geophys. Res.*, 100(94), 8873–8892,
533 doi:doi:10.1029/94JD02950, 1995.
- 534 Guenther, A., Geron, C., Pierce, T., Lamb, B., Harley, P. and Fall, R.: Natural emissions of non-methane
535 volatile organic compounds, carbon monoxide, and oxides of nitrogen from North America, *Atmos. Environ.*,
536 34(12–14), 2205–2230, doi:10.1016/S1352-2310(99)00465-3, 2000.
- 537 Hao, L. Q., Romakkaniemi, S., Yli-Pirilä, P., Joutsensaari, J., Kortelainen, A., Kroll, J. H., Miettinen, P.,
538 Vaattovaara, P., Tiitta, P., Jaatinen, A., Kajos, M. K., Holopainen, J. K., Heijari, J., Rinne, J., Kulmala, M.,
539 Worsnop, D. R., Smith, J. N. and Laaksonen, A.: Mass yields of secondary organic aerosols from the
540 oxidation of α -pinene and real plant emissions, *Atmos. Chem. Phys.*, 11(4), 1367–1378, doi:10.5194/acp-11-
541 1367-2011, 2011.
- 542 Henry, K. M., Lohaus, T. and Donahue, N. M.: Organic Aerosol Yields from α -Pinene Oxidation: Bridging
543 the Gap between First-Generation Yields and Aging Chemistry, *Environ. Sci. Technol.*, 46(22), 12347–
544 12354, doi:10.1021/es302060y, 2012.

- 545 Jacobson, M. Z.: Numerical techniques to solve condensational and dissolutional growth equations when
546 growth is coupled to reversible reactions, *Aerosol Sci. Technol.*, 27(4), 491–498,
547 doi:10.1080/02786829708965489, 1997.
- 548 Jenkin, M. E., Saunders, S. M. and Pilling, M. J.: The tropospheric degradation of volatile organic
549 compounds: A protocol for mechanism development, *Atmos. Environ.*, 31(1), 81–104, doi:10.1016/S1352-
550 2310(96)00105-7, 1997.
- 551 Jenkin, M. E., Young, J. C. and Rickard, A. R.: The MCM v3.3.1 degradation scheme for isoprene, *Atmos.*
552 *Chem. Phys.*, 15(20), 11433–11459, doi:10.5194/acp-15-11433-2015, 2015.
- 553 Jenkin, M. E., Wyche, K. P., Evans, C. J., Carr, T., Monks, P. S., Alfarra, M. R., Barley, M. H., McFiggans,
554 G. B., Young, J. C. and Rickard, A. R.: Development and chamber evaluation of the MCM v3.2 degradation
555 scheme for β -caryophyllene, *Atmos. Chem. Phys.*, 12(11), 5275–5308, doi:10.5194/acp-12-5275-2012, 2012.
- 556 Jenkin, M. E., Valorso, R., Aumont, B. and Rickard, A. R.: Estimation of rate coefficients and branching ra-
557 tios for reactions of organic peroxy radicals for use in automated mechanism construction, *Atmos. Chem.*
558 *Phys. Discuss.*, (February), 1–46, doi:10.5194/acp-2019-44, 2019.
- 559 Jokinen, T., Berndt, T., Makkonen, R., Kerminen, V.-M., Junninen, H., Paasonen, P., Stratmann, F.,
560 Herrmann, H., Guenther, A. B., Worsnop, D. R., Kulmala, M., Ehn, M. and Sipilä, M.: Production of
561 extremely low volatile organic compounds from biogenic emissions: Measured yields and atmospheric
562 implications, *Proc. Natl. Acad. Sci.*, 112(23), 7123–7128, doi:10.1073/pnas.1423977112, 2015.
- 563 Kanakidou, M., Seinfeld, J. H., Pandis, S. N., Barnes, I., Dentener, F. J., Facchini, M. C. and Dingenen, R.
564 Van: Organic aerosol and global climate modelling: a review, , 1053–1123, 2005.
- 565 Kang, E. and Root, M. J.: Introducing the concept of Potential Aerosol Mass (PAM), *Atmos. Chem. Phys.*,
566 (7), 5727–5744
- 567 Keywood, M. D., Varutbangkul, V., Bahreini, R., Flagan, R. C. and Seinfeld, J. H.: Secondary organic aerosol
568 formation from the ozonolysis of cycloalkenes and related compounds, *Environ. Sci. Technol.*, 38(15), 4157–
569 4164, doi:10.1021/es035363o, 2004.
- 570 Korhonen, H., Lehtinen, K. E. J. and Kulmala, M.: Atmospheric Chemistry and Physics Multicomponent
571 aerosol dynamics model UHMA: model development and validation, *Atmos. Chem. Phys.*, 4, 757–771,
572 doi:10.1002/erv.2305, 2004.
- 573 Kristensen, K., Cui, T., Zhang, H., Gold, A., Glasius, M. and Surratt, J. D.: Dimers in α -pinene secondary
574 organic aerosol: Effect of hydroxyl radical, ozone, relative humidity and aerosol acidity, *Atmos. Chem. Phys.*,
575 14(8), 4201–4218, doi:10.5194/acp-14-4201-2014, 2014.
- 576 Kristensen, K., Jensen, L. N., Glasius, M. and Bilde, M.: The effect of sub-zero temperature on the formation
577 and composition of secondary organic aerosol from ozonolysis of alpha-pinene, *Environ. Sci. Process.*
578 *Impacts*, 19(10), 1220–1234, doi:10.1039/c7em00231a, 2017.
- 579 Kroll, J. H., Ng, N. L., Murphy, S. M., Flagan, R. C. and Seinfeld, J. H.: Secondary organic aerosol formation
580 from isoprene photooxidation under high-NO_x conditions, *Geophys. Res. Lett.*, 32(18), 1–4,
581 doi:10.1029/2005GL023637, 2005.
- 582 Lambe, A. T., Onasch, T. B., Massoli, P., Croasdale, D. R., Wright, J. P., Ahern, A. T., Williams, L. R.,
583 Worsnop, D. R., Brune, W. H. and Davidovits, P.: Laboratory studies of the chemical composition and cloud
584 condensation nuclei (CCN) activity of secondary organic aerosol (SOA) and oxidized primary organic aerosol
585 (OPOA), *Atmos. Chem. Phys.*, 11(17), 8913–8928, doi:10.5194/acp-11-8913-2011, 2011.

- 586 Lambe, A. T., Chhabra, P. S., Onasch, T. B., Brune, W. H., Hunter, J. F., Kroll, J. H., Cummings, M. J.,
587 Brogan, J. F., Parmar, Y., Worsnop, D. R., Kolb, C. E. and Davidovits, P.: Effect of oxidant concentration,
588 exposure time, and seed particles on secondary organic aerosol chemical composition and yield, *Atmos.*
589 *Chem. Phys.*, 15(6), 3063–3075, doi:10.5194/acp-15-3063-2015, 2015.
- 590 Lee, A., Goldstein, A. H., Keywood, M. D., Gao, S., Varutbangkul, V., Bahreini, R., Ng, N. L., Flagan, R. C.
591 and Seinfeld, J. H.: Gas-phase products and secondary aerosol yields from the ozonolysis of ten different
592 terpenes, *J. Geophys. Res. Atmos.*, 111(7), 1–18, doi:10.1029/2005JD006437, 2006.
- 593 Liu, J., D'Ambro, E. L., Lee, B. H., Lopez-Hilfiker, F. D., Zaveri, R. A., Rivera-Rios, J. C., Keutsch, F. N.,
594 Iyer, S., Kurten, T., Zhang, Z., Gold, A., Surratt, J. D., Shilling, J. E. and Thornton, J. A.: Efficient Isoprene
595 Secondary Organic Aerosol Formation from a Non-IEPOX Pathway, *Environ. Sci. Technol.*, 50(18), 9872–
596 9880, doi: 10.1021/acs.est.6b01872, 2016.
- 597 Miller, K. A., Siscovick, D. S., Sheppard, L., Shepherd, K., Sullivan, J. H., Anderson, G., L. and Kaufman J.
598 D.: Long-Term Exposure to Air Pollution and Incidence of Cardiovascular Events in Women, *N. Engl. J.*
599 *Med.*, 356(5), 447–458, doi:10.1002/anie.201206370, 2007.
- 600 Nannoolal, Y., Rarey, J. and Ramjugernath, D.: Estimation of pure component properties part 3. Estimation of
601 the vapor pressure of non-electrolyte organic compounds via group contribution and group interactions, *Fluid*
602 *Phase Equilib.*, 269(1–2), 117–133, doi: 10.1016/j.fluid.2008.04.020, 2008.
- 603 Nah, T., Sanchez, J., Boyd, C. M. and Ng, N. L.: Photochemical Aging of α -pinene and β -pinene Secondary
604 Organic Aerosol formed from Nitrate Radical Oxidation, *Environ. Sci. Technol.*, 50(1), 222–231,
605 doi:10.1021/acs.est.5b04594, 2016.
- 606 Ng, N. L. and Chhabra, P. S.: Effect of NO_x level on secondary organic aerosol (SOA) formation from the
607 photooxidation of terpenes, *Atmos. Chem. Phys.*, (7), 5159–5174, doi: 10.1016/j.cub.2015.10.018, 2007.
- 608 Öström, E., Putian, Z., Schurgers, G., Mishurov, M., Kivekäs, N. and Lihavainen, H.: Modeling the role of
609 highly oxidized multifunctional organic molecules for the growth of new particles over the boreal forest re-
610 gion, , 8887–8901, 2017.
- 611 Pankow, J. F. and Asher, W. E.: SIMPOL.1: a simple group contribution method for predicting vapor
612 pressures and enthalpies of vaporization of multifunctional organic compounds, *Rev. Mex. Ciencias Farm.*,
613 (8), 2773–2796, doi:doi: 10.5194/acp-8-2773-2008, 2008.
- 614 Pathak, R., Donahue, N. M. and Pandis, S. N.: Ozonolysis of β -pinene: Temperature dependence of secondary
615 organic aerosol mass fraction, *Environ. Sci. Technol.*, 42(14), 5081–5086, doi:10.1021/es070721z, 2008.
- 616 Pathak, R. K., Stanier, C. O., Donahue, N. M. and Pandis, S. N.: Ozonolysis of α -pinene at atmospherically
617 relevant concentrations: Temperature dependence of aerosol mass fractions (yields), *J. Geophys. Res. Atmos.*,
618 112(3), 1–8, doi:10.1029/2006JD007436, 2007.
- 619 Presto, A. A., Huff Hartz, K. E. and Donahue, N. M.: Secondary organic aerosol production from terpene
620 ozonolysis. 2. Effect of NO_x concentration, *Environ. Sci. Technol.*, 39(18), 7046–7054,
621 doi:10.1021/es050400s, 2005.
- 622 Qi, X., Ding, A., Roldin, P., Xu, Z., Zhou, P., Sarnela, N., Nie, W., Huang, X., Rusanen, A., Ehn, M., Rissa-
623 nen, M. P., Petäjä, T., Kulmala, M. and Boy, M.: Modelling studies of HOMs and their contributions to new
624 particle formation and growth: Comparison of boreal forest in Finland and a polluted environment in China,
625 *Atmos. Chem. Phys.*, 18(16), 11779–11791, doi:10.5194/acp-18-11779-2018, 2018.

- 626 Quéléver, L. L. J., Kristensen, K., Jensen, L., Rosati, B., Teiwes, R., Daellenbach, K. R., Peräkylä, O., Roldin,
627 P., Pedersen, H. B., Glasius, M., Bilde, M., and Ehn, M.: Effect of temperature on the formation of Highly-
628 oxygenated Organic Molecules (HOM) from alpha-pinene ozonolysis, *Atmos. Chem. Phys. Discuss.*,
629 <https://doi.org/10.5194/acp-2018-1276>, in review, 2018.
- 630 Roldin P., Ehn, M, Kurtén, T., Olenius, T., Rissanen, M.P., Sarnela, N., Elm, J., Rantala, P., Hao, L.,
631 Hyttinen, N., Heikkinen, L., Worsnop, D. R., Pichelstorfer, L., Xavier, C., Clusius, P., Öström, E., Petäjä, T.,
632 Kulmala, M., Vehkamäki, H., Virtanen, A., Riipinen, I., and Boy, M., The role of highly oxygenated organic
633 molecules in the Boreal aerosol-cloud-climate system, *Nature Communications*, under review 2019.
- 634 Rosenfeld, D., Andreae, M. O., Asmi, A., Chin M., De Leeuw, G., Donovan, D. P., Kahn, R, Kinne, S.,
635 Kivekäs, N., Kulmala, M., Lau W., Schmidt K, S., Suni T., Wagner T., Wild, M., and Quaas J., Global obser-
636 vations of aerosol-cloud-precipitation-climate interactions, *Rev. Geophys.*, 52, 750–808,
637 [doi:10.1002/2013RG000441](https://doi.org/10.1002/2013RG000441).
- 638 Saathoff, H. and Naumann, K.-H.: Temperature dependence of yields of secondary organic aerosols from the
639 ozonolysis of α -pinene and limonene, *Atmos. Chem. Phys.*, (March), 4–15, [doi:10.5194/acp-9-1551-2009](https://doi.org/10.5194/acp-9-1551-2009),
640 2009.
- 641 Sarrafzadeh, M., Wildt, J., Pullinen, I., Springer, M., Kleist, E., Tillmann, R., Schmitt, S. H., Wu, C., Mentel,
642 T. F., Zhao, D., Hastie, D. R. and Kiendler-Scharr, A.: Impact of NO_x and OH on secondary organic aerosol
643 formation from β -pinene photooxidation, *Atmos. Chem. Phys.*, 16(17), 11237–11248, [doi:10.5194/acp-16-](https://doi.org/10.5194/acp-16-11237-2016)
644 [11237-2016](https://doi.org/10.5194/acp-16-11237-2016), 2016.
- 645 Saunders, S. M., Jenkin, M. E., Derwent, R. G. and Pilling, M. J.: Protocol for the development of the Master
646 Chemical Mechanism, MCM v3 (Part A): Tropospheric degradation of non-aromatic volatile organic
647 compounds, *Atmos. Chem. Phys.*, 3(1), 161–180, [doi:10.5194/acp-3-161-2003](https://doi.org/10.5194/acp-3-161-2003), 2003.
- 648 Schmale, J., Henning, S., Henzing, B., Keskinen, H., Sellegri, K., Ovadnevaite, J., Bougiatioti, A., Kalivitis,
649 N., Stavroulas, I., Jefferson, A., Park, M., Schlag, P., Kristensson, A., Iwamoto, Y., Pringle, K., Reddington,
650 C., Aalto, P., Äijälä, M., Baltensperger, U., Bialek, J., Birmili, W., Bukowiecki, N., Ehn, M., Fjærraa, A. M.,
651 Fiebig, M., Frank, G., Fröhlich, R., Frumau, A., Furuya, M., Hammer, E., Heikkinen, L., Herrmann, E.,
652 Holzinger, R., Hyono, H., Kanakidou, M., Kiendler-Scharr, A., Kinouchi, K., Kos, G., Kulmala, M.,
653 Mihalopoulos, N., Motos, G., Nenes, A., O’Dowd, C., Paramonov, M., Petäjä, T., Picard, D., Poulain, L.,
654 Prévôt, A. S. H., Slowik, J., Sonntag, A., Swietlicki, E., Svenningsson, B., Tsurumaru, H., Wiedensohler, A.,
655 Wittbom, C., Ogren, J. A., Matsuki, A., Yum, S. S., Myhre, C. L., Carslaw, K., Stratmann, F. and Gysel, M.:
656 Corrigendum: Collocated observations of cloud condensation nuclei, particle size distributions, and chemical
657 composition, *Sci. data*, 5, 180094, [doi:10.1038/sdata.2018.94](https://doi.org/10.1038/sdata.2018.94), 2018.
- 658 Shilling, J. E.: Particle mass yield in secondary organic aerosol formed by the dark ozonolysis of α -pinene,
659 *Atmos. Chem. Phys.*, 8(1992), 2073–2088, 2008.
- 660 Stirnweis, L., Marcolli, C., Dommen, J., Barmet, P., Frege, C., Platt, S. M., Bruns, E. A., Krapf, M., Slowik,
661 J. G., Wolf, R., Prévôt, A. S. H., Baltensperger, U. and El-Haddad, I.: Assessing the influence of NO_x con-
662 centrations and relative humidity on secondary organic aerosol yields from α -pinene photo-oxidation through
663 smog chamber experiments and modelling calculations, *Atmos. Chem. Phys.*, 17(8), 5035–5061, [doi:10.5194/](https://doi.org/10.5194/acp-17-5035-2017)
664 [acp-17-5035-2017](https://doi.org/10.5194/acp-17-5035-2017), 2017.
- 665 Tasoglou, A. and Pandis, S. N.: Formation and chemical aging of secondary organic aerosol during the β -
666 caryophyllene oxidation, *Atmos. Chem. Phys.*, 15(11), 6035–6046, [doi:10.5194/acp-15-6035-2015](https://doi.org/10.5194/acp-15-6035-2015), 2015.
- 667 Topping, D.: UManSysProp v1.0: an online and open-source facility for molecular property prediction and
668 atmospheric aerosol calculations, , 899–914, [doi:10.5281/zenodo.45143](https://doi.org/10.5281/zenodo.45143), 2016.

- 669 Waring, M. S.: Secondary organic aerosol formation by limonene ozonolysis: Parameterizing multi-
670 generational chemistry in ozone- and residence time-limited indoor environments, *Atmos. Environ.*, 144, 79–
671 86, doi:<https://doi.org/10.1016/j.atmosenv.2016.08.051>, 2016.
- 672 Zhao, D., Schmitt, S. H., Wang, M., Acir, I. H., Tillmann, R., Tan, Z., Novelli, A., Fuchs, H., Pullinen, I.,
673 Wegener, R., Rohrer, F., Wildt, J., Kiendler-Scharr, A., Wahner, A. and Mentel, T. F.: Effects of NO_x and
674 SO₂ on the secondary organic aerosol formation from photooxidation of α -pinene and limonene, *Atmos.*
675 *Chem. Phys.*, 18(3), 1611–1628, doi:10.5194/acp-18-1611-2018, 2018.
- 676 Zhao, D. F., Kaminski, M., Schlag, P., Fuchs, H., Acir, I. H., Bohn, B., Häseler, R., Kiendler-Scharr, A.,
677 Rohrer, F., Tillmann, R., Wang, M. J., Wegener, R., Wildt, J., Wahner, A. and Mentel, T. F.: Secondary
678 organic aerosol formation from hydroxyl radical oxidation and ozonolysis of monoterpenes, *Atmos. Chem.*
679 *Phys.*, 15(2), 991–1012, doi:10.5194/acp-15-991-2015, 2015.